AIAA 02–3160

Numerical Simulations of Vortex Generator Vanes and Jets on a Flat Plate

Brian G. Allan
ICASE, Hampton, VA 23681
Chung-Sheng Yao and John C. Lin
NASA Langley Research Center, Hampton, VA 23681

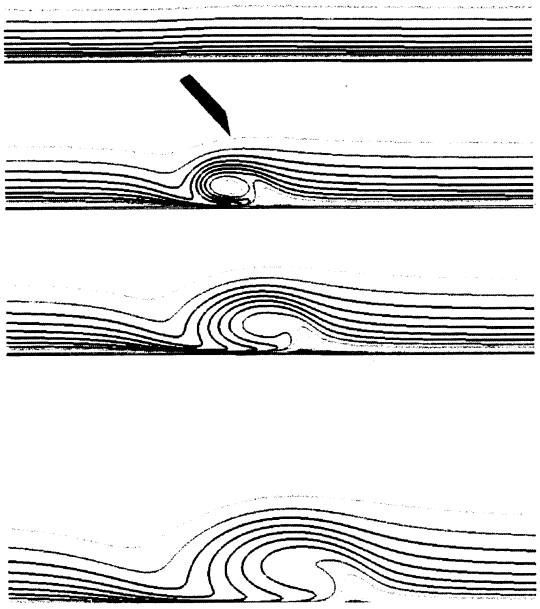

1st AIAA Flow Control Conference
June 24–27, 2002/St. Louis, MO

Numerical Simulations of Vortex Generator Vanes and Jets on a Flat Plate

Brian G. Allan*
ICASE, Hampton, VA 23681

Chung-Sheng Yao† and John C. Lin‡
NASA Langley Research Center, Hampton, VA 23681

Numerical simulations of a single low-profile vortex generator vane, which is only a small fraction of the boundary-layer thickness, and a vortex generating jet have been performed for flows over a flat plate. The numerical simulations were computed by solving the steady-state solution to the Reynolds-averaged Navier-Stokes equations. The vortex generating vane results were evaluated by comparing the strength and trajectory of the streamwise vortex to experimental particle image velocimetry measurements. From the numerical simulations of the vane case, it was observed that the Shear-Stress Transport (SST) turbulence model resulted in a better prediction of the streamwise peak vorticity and trajectory when compared to the Spalart-Allmaras (SA) turbulence model. It is shown in this investigation that the estimation of the turbulent eddy viscosity near the vortex core, for both the vane and jet simulations, was higher for the SA model when compared to the SST model. Even though the numerical simulations of the vortex generating vane were able to predict the trajectory of the streamwise vortex, the initial magnitude and decay of the peak streamwise vorticity were significantly under predicted. A comparison of the positive circulation associated with the streamwise vortex showed that while the numerical simulations produced a more diffused vortex, the vortex strength compared very well to the experimental observations. A grid resolution study for the vortex generating vane was also performed showing that the diffusion of the vortex was not a result of insufficient grid resolution. Comparisons were also made between a fully modeled trapezoidal vane with finite thickness to a simply modeled rectangular thin vane. These comparisons showed that the simply modeled rectangular vane produced a streamwise vortex which had a strength and trajectory very similar to the fully modeled trapezoidal vane.

Nomenclature

h	Vane height
Re_x	Reynolds number based on length x
U_∞	Freestream Velocity, m/s
u, v, w	Velocity in x, y, z directions respectively, m/s
VR	Velocity ratio, $(= V_{jet}/U_\infty)$
x, y, z	Cartesian axes
Γ^+	Positive circulation
α	Vortex generator vane angle-of-attack, degrees
μ_t	Turbulent eddy viscosity
δ	Boundary layer height
ω_x	Streamwise Vorticity, $(= \partial w/\partial y - \partial v/\partial z)$, $1/s$

Introduction

Incorporation of vortex generating (VG) devices, in the design of compact aircraft inlets, has demonstrated significant improvements in turbofan engine-face flow distortion.[1] Recently Hamstra et al.[1] have shown a comparison between a computational fluid dynamics (CFD) analysis of a compact inlet flow, with VG vanes, to experimental results. They demonstrated how a CFD analysis was able to accurately predict the inlet surface pressure and engine-face flow distortion. These CFD simulations used a simplified model of the VG vane, described by Bender et al.,[2] eliminating the need to model the vane geometry resulting in a reduced computational cost.

The model described by Bender et al.[2] models a VG vane by introducing a source term in the momentum and energy equations. The strength of the source term is adjusted based on the local flow and represents the side force generated by a vane or row of vanes. The success of this model for internal inlet flows shows that it may be possible to simulate the effects of VG vanes for other types of flows using a boundary condition approach rather than fully gridding the flow control devices. The validation of the Bender et al.[2] model was made using an integral of the cross flow kinetic energy far down stream of the vanes at the inlet exit. In an effort to achieve a more detail evaluation of this and other types of reduced CFD models for vortex generator devices, numerical simulations of a single VG vane and VG jet on a flat plate were performed.

The numerical simulations of a single vane on a flat plate were generated in collaboration with the wind tunnel experiments performed at NASA Langley. This experi-

*ICASE, Mail Stop 132C, NASA Langley Research Center, Hampton, VA 23681 (email: allan@icase.edu). This research was supported by the National Aeronautics and Space Administration under NASA Contract No. NAS1-97046 while the author was in residence at the ICASE, NASA Langley Research Center, Hampton, VA 23681-2199. AIAA member

†NASA Langley Research Center, Mail Stop 170, Hampton, VA 23681.

‡NASA Langley Research Center, Mail Stop 170, Hampton, VA 23681, AIAA Asociate Fellow.

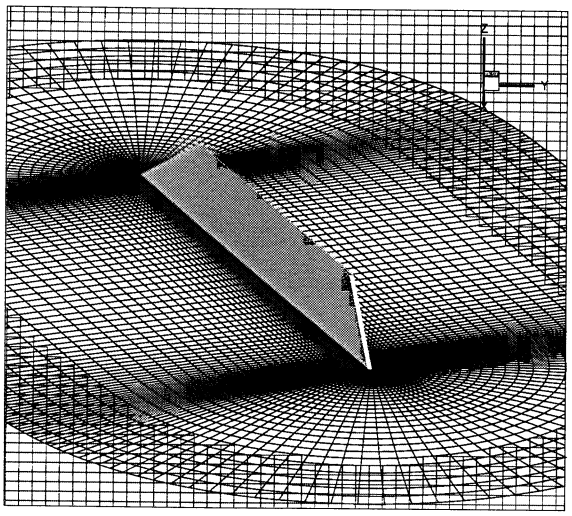

Fig. 1 Overset grids for the trapezoidal vortex generator vane.

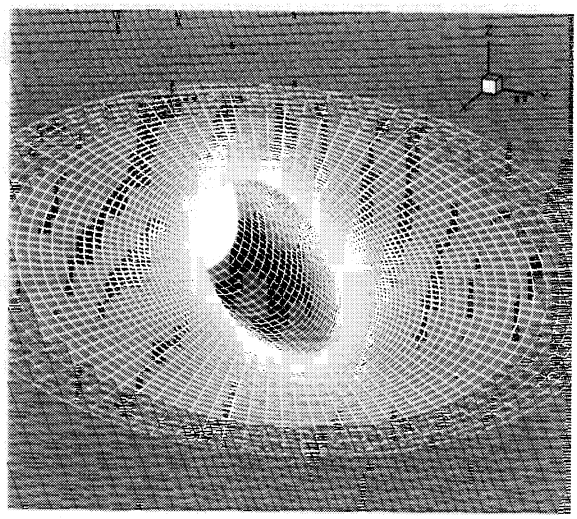

Fig. 2 Close-up view of the overset nozzle grids used in the vortex generator jet simulation.

mental data will be used to assess the flow predicted by a Reynolds-averaged Navier-Stokes flow solver for a single VG vane case. Evaluation of the numerical and experimental data will provide detailed insight into the physics of the flow around and downstream of the VG vane. The insight gained from this investigation can then be used to justify future modeling choices for the development of a reduced ordered CFD model.

Numerical Modeling

The steady-state flow field about a single vortex generator vane and a steady jet on a flat plate were computed using the flow solver code, OVERFLOW,[3,4] developed at NASA. This code solves the compressible Reynolds-averaged Navier-Stokes (RANS) equations using the diagonal scheme of Pulliam and Chaussee.[5] The RANS equations are solved on structured grids using the overset grid framework of Steger et al.[6] This overset grid framework allows for the use of structured grids for problems which have complex geometries. To improve the convergence of the steady-state solution, the OVERFLOW code also includes a low-Mach preconditioning option and a multigrid acceleration routine, which were both used for the numerical simulations.

The OVERFLOW code has several options for turbulence models. This investigation focuses on the one-equation model of Spalart and Allmaras[7] (SA) and the two-equations (k-ω) Shear-Stress Transport (SST) model of Menter.[8] The SA turbulence model is popular because of its ease of implementation, relative low cost, and good performance. The SST model is a k-ω two-equation model which accounts for the transport of the principal shear stress in adverse pressure gradients boundary layers. Both models are well known and have been widely used for aerospace vehicle applications.

The numerical simulations were performed using the parallel version of the OVERFLOW code developed by Jespersen.[9] This code uses the Message-Passing Interface (MPI) and can run on a tightly-coupled parallel machine or a network of workstations. The code distributes zones to individual processors and can split larger individual zones across multiple processors by using a pipelined Gaussian elimination method. Splitting the larger zones across multiple processors significantly improves the load-balancing for problems with zones of varying size.

The structured overset grid system was generated using the Chimera Grid Tools package.[10] Figure 1 shows a close-up view of the overset grids near the trapezoidal vane on the flat plate. This vane was modeled with a finite thickness and rounded edges using an O-grid around the vane and a cap grid for the top edge of the vane. The O-grid is overset on a Cartesian block grid which models the flat plate. In Fig. 1 a blanked out region on the flat plate grid can be seen where the the flow field is resolved by the finer vane grids. The volume grids around the vane were generated using the hyperbolic grid generator program in the Chimera Grid Tools package.

Figure 2 shows a close-up view of the nozzle grid system for the vortex generator jet simulation. The steady jet is skewed 90^o to the freestream flow and pitched at an inclined angle of 15^o to the surface. These pitch and skew angles for the jet result in the generation of a single streamwise vortex. This jet is simulated by modeling the nozzle below the surface of the flat plate. This simplifies the inflow boundary condition for the jet by letting the flow develop in the nozzle and exiting at the flat plate surface.

Wind Tunnel Experiments

Wind tunnel experiments of a single vane submerged within a turbulent boundary layer over a flat plate were conducted in NASA Langley's 20 × 28-Inch Shear Flow Tunnel. Detailed flow field velocity measurements were taken in crossflow planes downstream of the VG device

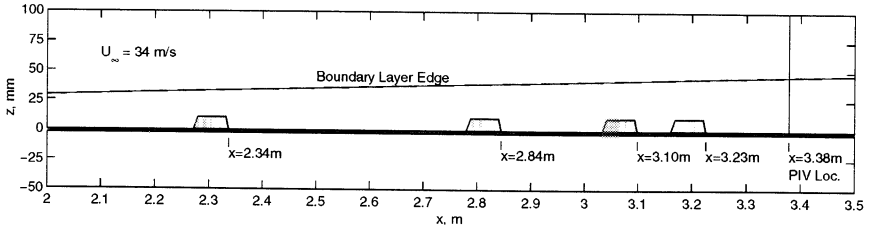

Fig. 3 Location of VG vanes and the PIV measurement plane. This figure also shows the boundary layer edge with respect to the vane device height.

using a three-dimensional stereo digital Particle Image Velocimetry (PIV) system, where all three components of velocity were obtained through stereoscopic vector reconstruction, as describe by Yao et al.[11] The assembly of this PIV flow field data, for various distances downstream of the VG vane, is then used to characterize the evolution of the streamwise vortex embedded in a boundary layer.

The experiments were conducted at a freestream velocity, U_∞, of 34 m/s. A splitter plate was mounted above the test section floor and its leading edge was tripped to force a fully developed turbulent boundary layer downstream. The PIV data was taken at a fixed crossflow plane station located 3.38 m downstream from the leading edge of the plate. Four flow field surveys were taken, where each survey consisted of placing an individual VG at a different position, upstream of the PIV measuring location. Figure 3 shows the location of the PIV measuring station ($x = 3.38\ m$) as well as the four VG locations at $x = 3.23\ m$, 3.10 m, 2.84 m, and 2.34 m that correspond to a distance of 15.2 cm, 27.9 cm, 53.3 cm, and 104 cm from the vane trailing edge to the measurement location, respectively. This figure also shows the relative height of the boundary layer for the baseline flat plate flow without a VG device.

The baseline boundary-layer thickness, δ, at the vane locations varies from 33 mm, at the most upstream location ($x = 2.34\ m$), to 45 mm, the farthest downstream vane location ($x = 3.23m$). The VG vane used for this experiment has a height, h, of 10.2 mm, which results in a variation of h/δ between 0.31 and 0.23. The vane has a length, L, of 71 mm resulting in a L/h of 7. The vane has a trapezoidal planform geometry similar in shape to that of the trapezoidal wing-micro VGs reported by Lin.[12]

Using this type of experimental setup the boundary layer thickness and velocity profile vary at the four different VG locations. The objective of this study is to characterize the trajectory of the streamwise vortex and the flow field downstream of the VG vane. Thus, this variation in the boundary layer profile is unwanted. It will be shown later that this variation has a small effect on the data point for the most upstream vane location and a very slight effect on the data points for the other three VG locations.

Results and Discussions

Numerical simulations of the vortex generating vane and jet on a flat plate are performed. Two simulations of the a single vane at 23° and 10° angles-of-attack are computed and compared to experimental data. A numerical simulation of a vortex generating jet is also performed and compared to the results of the vane. Both vortex generating devices are characterized by the trajectory of the streamwise vortex core, the decay of the peak vorticity, and the circulation strength of the vortex.

Experimental Results

The PIV system collected flow filed data on a grid which had 40 points in the spanwise direction and 33 points in the vertical direction. The data points were evenly spaced at approximately 1.7 mm in the vertical direction and 2.2 mm in the spanwise direction. The three components of mean velocity were then collected at each grid point by the PIV system. Using the velocity data, the streamwise component of the vorticity was computed. The streamwise vorticity data was then used to plot the trajectory and decay of the peak vorticity as well as the positive circulation. This data was then used to evaluate the numerical results given below.

Vortex Generating Vane

The finite thickness trapezoidal vane shown in Fig. 1 models the shape and thickness of the actual vane used in the wind tunnel experiments. This model of the vane was used to simulate the flow of the vane on a flat plate at 23° and 10° angle-of-attack using a freestream velocity of $34 m/s$. Numerical simulations are made using both SA and SST turbulence models. Unlike the experiments, the numerical simulations will evaluate the trajectory of the streamwise vortex by positioning the vane at a single ($x = 3.23\ m$) location. The flow from this vane location is then compared to the experimental data. The error introduced by this approach will be quantified by comparing the numerical simulations for each vane location.

Figure 4 shows a comparison of the peak streamwise vorticity for the 23° vane case between the experimental data and the numerical simulations using the SA and SST turbulence models. Comparing the magnitude of the peak vorticity, it can be seen that both simulations under predict the initial magnitude and decay rates. The SST and SA simulations both predict an initial peak vorticity which are almost the same. However the SA simulation shows a much faster decay of the peak vorticity as compared to the SST simulation.

The path of the vortex core for the 23° vane case is

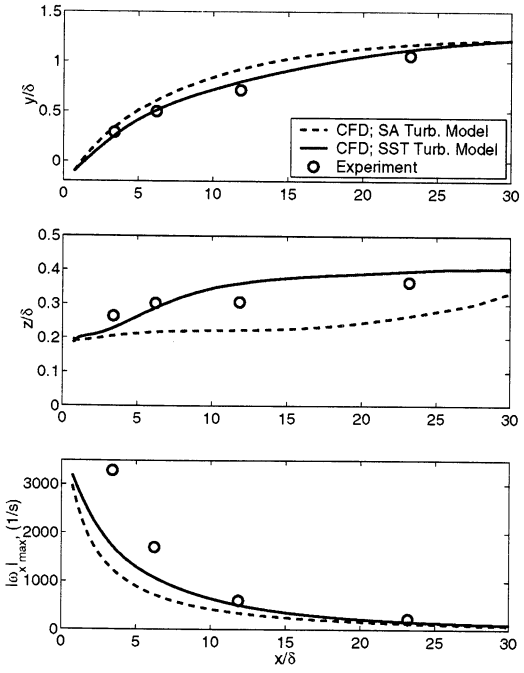

Fig. 4 Trajectory and magnitude comparisons of the peak streamwise vorticity, using the SA and SST turbulence models, to the experimental data for the vane at $\alpha = 23^o$ where $\delta = 45mm$.

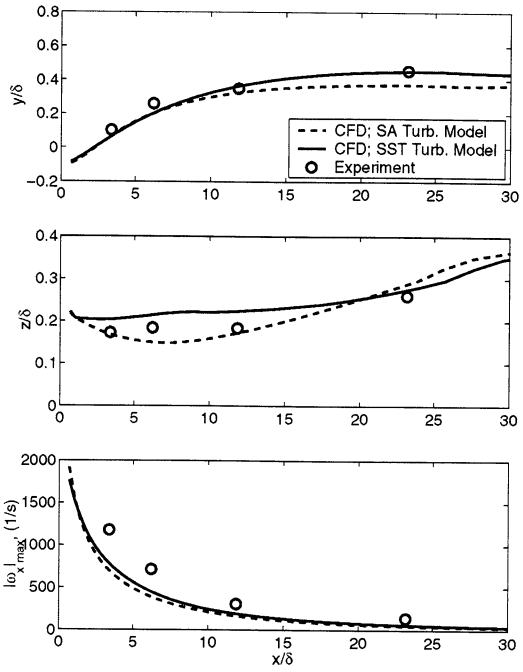

Fig. 5 Trajectory and magnitude comparisons of the peak streamwise vorticity, using the SA and SST turbulence models, to the experimental data for the vane at $\alpha = 10^o$ where $\delta = 45mm$.

shown in Fig. 4. The spanwise, y, trajectory of the vortex core shows that the SST simulation compares very well with the experiment and that the SA model tends to over predict the path in the cross flow direction. The location of the center of the vortex in the vertical direction, z, shows that both simulations have a hard time predicting the vertical trajectory. The SST model compares well with the experiments up to $x/\delta = 5$ and does not capture the vertical jump in the vortex location at $x/\delta = 10$ as seen in the experimental data. Figure 4 shows how the SA model under predicts the vertical location of the center of the vortex.

Using the SA and SST turbulence models, the flow about a single vane at 10° angle-of-attack was computed. The magnitude and trajectory of the peak core vorticity are shown in Fig. 5 with a comparison to the experimental data. This comparison shows similar trends as seen in the 23° vane case. The vertical location of the vortex center does compare well to the experimental data for both the SST and SA models. The spanwise path of the vortex compares very well with the experiment when using the SST model and is slightly under predicted for the SA simulation. The magnitude of the peak vorticity is still under predicted by the numerical simulations when compared to the experimental data. Unlike the 23° vane case, the peak vorticity predicted by the SA simulation is only slightly lower than the peak vorticity for the SST simulation.

Positive Circulation

The positive circulation, Γ^+, about the streamwise vortex was computed for the 23° and 10° vane cases and shown in Figs. 6 and 7. The circulation was computed by integrating the positive streamwise vorticity around the vortex. In and effort to make a fair comparison between the numerical and experimental data, the velocity field was interpolated onto a grid similar in resolution as the experimental PIV data. The positive circulation about the streamwise vortex was then computed using this interpolated velocity data by computing vorticity and then integrating.

Figure 6 shows a comparison of the positive circulation between the numerical simulations and the experimental data for the $\alpha = 23°$ case. This comparison shows that the circulation computed from the experimental data is lower than the numerical simulation for the first two data points. The circulation values compare much better for the last two experimental data points. This figure also shows a comparison between the circulation for the SA and SST turbulence model simulations. This comparison shows that the circulation is about the same when using the SA and SST turbulence models. This result shows how simulations for both turbulence models generate a vortex of the similar strength and decay rates. The $\alpha = 10°$ case in Fig. 7 shows how the circulation from the experimental data compares well to the numerical simulations except for the first data point. This figure also shows how the circulation for the numerical simulations are almost the for the SA and SST turbulence models. As in the 23° case, the 10° case shows

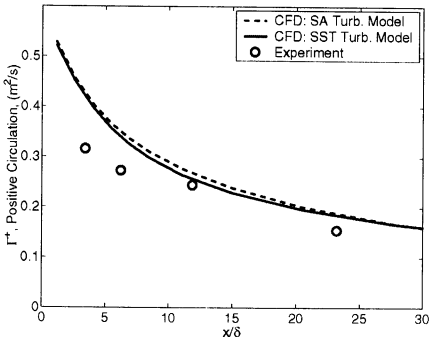

Fig. 6 Comparison of positive circulation for $\alpha = 23°$ where $\delta = 45mm$.

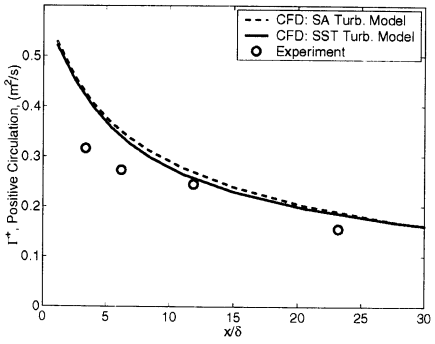

Fig. 7 Comparison of positive circulation for $\alpha = 10°$ where $\delta = 45mm$.

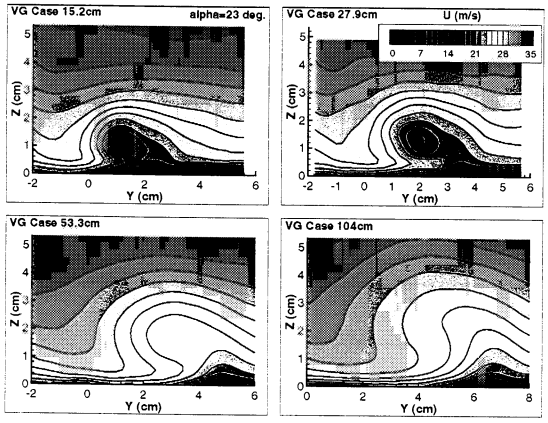

a) Experiment: Streamwise velocity contours, $\alpha = 23°$.

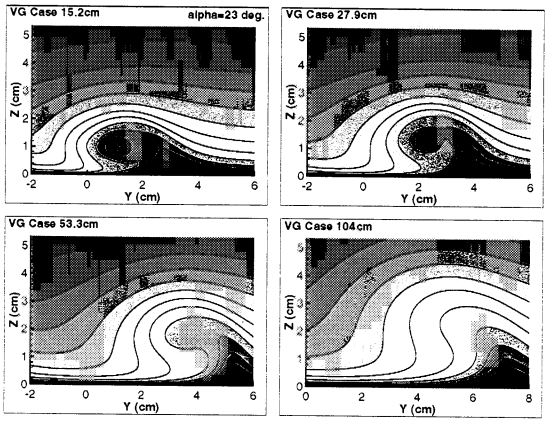

b) CFD: Streamwise velocity contours, $\alpha = 23°$.

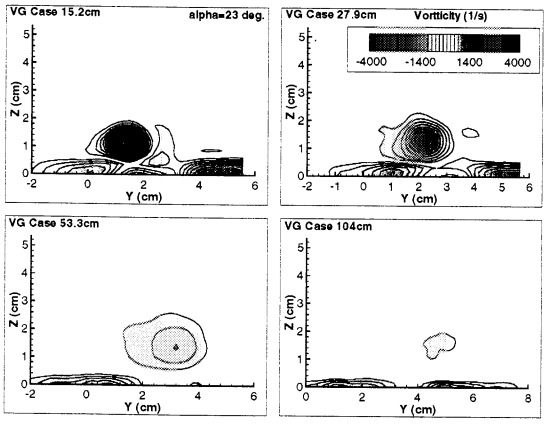

c) Experiment: Streamwise vorticity contours, $\alpha = 23°$.

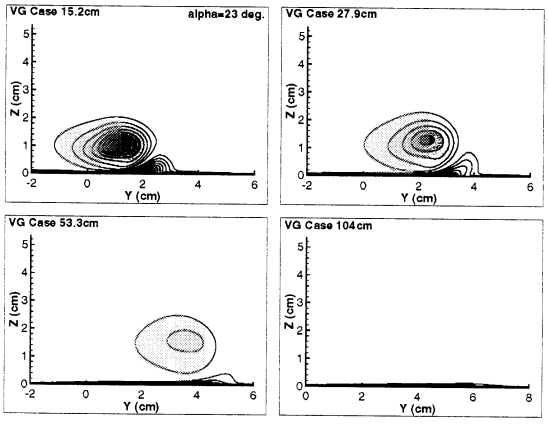

d) CFD: Streamwise vorticity contours, $\alpha = 23°$.

Fig. 8 A comparison between CFD and experiment for the 23° vane case at four different locations downstream of the vane.

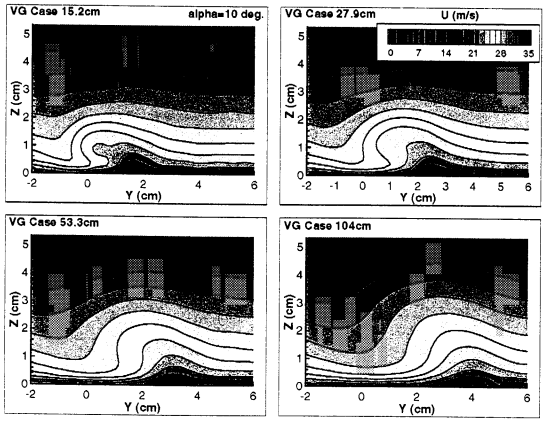

a) Experiment: Streamwise velocity contours, $\alpha = 10°$.

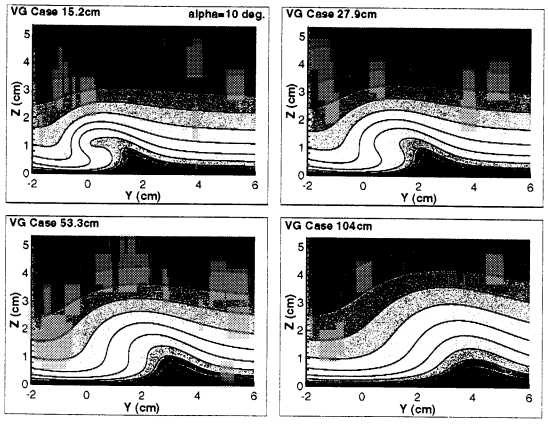

b) CFD: Streamwise velocity contours, $\alpha = 10°$.

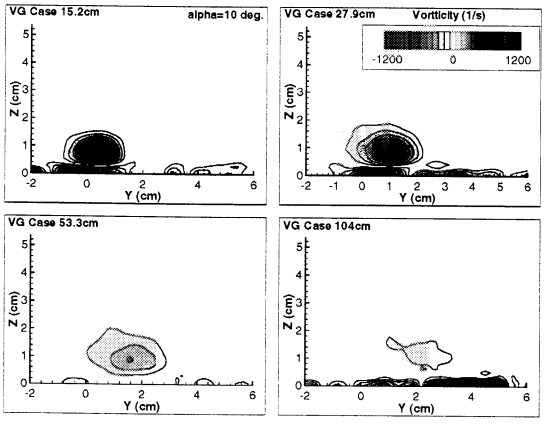

c) Experiment: Streamwise vorticity contours, $\alpha = 10°$.

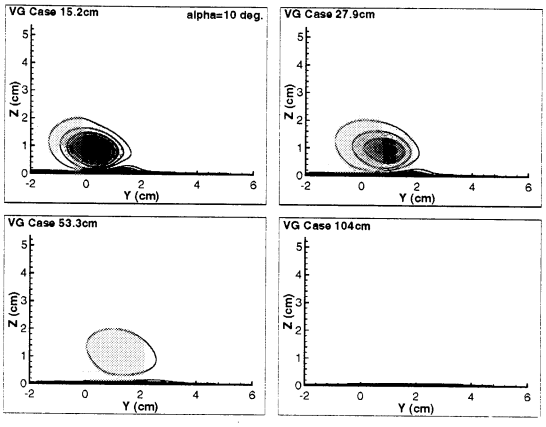

d) CFD: Streamwise vorticity contours, $\alpha = 10°$.

Fig. 9 A comparison between CFD and experiment for the $10°$ vane case at four different locations downstream of the vane.

the vortex strength and decay rate nearly the same when comparing the two turbulence models.

The comparison of circulation for the numerical simulations using the SA and SST turbulence models show how they both produce a streamwise vortex of the equal strength. This shows that the difference in the peak vorticity is not related to the initial strength of the streamwise vortex but instead to the diffusion of the vortex. Specifically, comparisons of the peak vorticity show how the SA model diffuses the streamwise vortex faster than the SST model. The peak vorticity also shows how the numerical simulations tend to diffuse the streamwise vortex significantly faster than was observed by the experimental results.

Figures 8 and 9 show the streamwise velocity and streamwise vorticity contours for the vortex generating vane at 23° and 10° angles-of-attack for the numerical simulations using the SST turbulence model and the experimental PIV data. The 23° case in Fig. 8 shows how the streamwise velocity is reduced at the core of the vortex. The streamwise velocity contours also show the vortex core inside the boundary layer where the top most contour line gives an estimate of the boundary layer edge. The velocity contours located 15.2 *cm* and 27.9 *cm* downstream from the vane show a vortex which is much more concentrated in the experiment data than in the numerical simulations. The velocity contours 53.3 *cm* and 104 *cm* downstream of the vane show a better comparison between the experiment and CFD. The streamwise vorticity contours also indicate a more concentrated vortex at 15.2 *cm* and 27.9 *cm* downstream for the experimental data as compared to the numerical results. The contour plots of vorticity also show a vortex which is much more circular for the experiment results than the vortex predicted by the numerical simulations. Going farther downstream, the vorticity contours at 53.3 *cm* and 104 *cm* from the vane compare much better where the magnitude of the peak vorticity, as was shown in Fig. 4, compares more favorably.

The contours for the 10° vane case are shown in Fig. 9 where the velocity and vorticity contours between the experiment and simulation compare better than the 23° vane case. There is a small difference in the streamwise velocity at the 15.2 *cm* and 27.9 *cm* downstream locations but overall the velocity contours compare well. The vorticity contours in Fig. 9 do show a more concentrated vortex at the 15.2 *cm* and 27.9 *cm* locations for the experiment as would be expected knowing the difference in the peak vor-

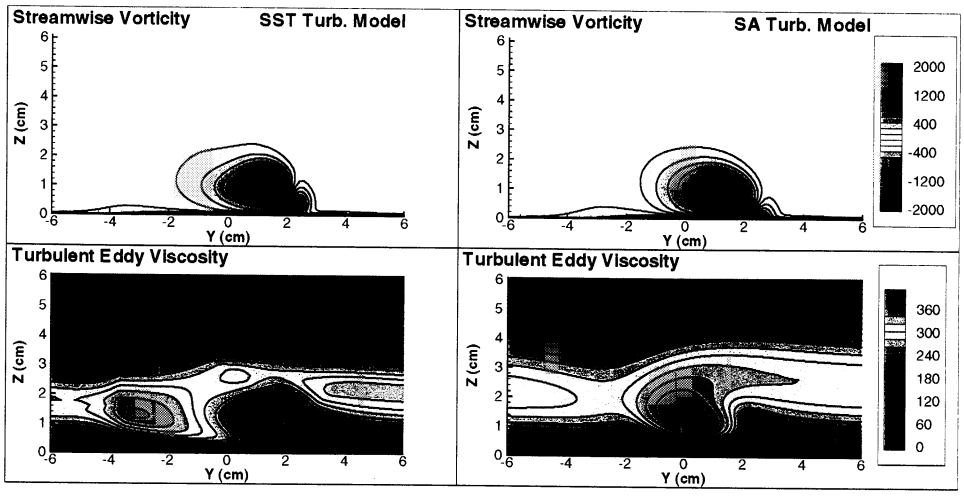

Fig. 10 Contour plots of the streamwise vorticity and the eddy viscosity for the fully modeled trapezoidal vane using the SA and SST turbulence models.

ticity given in Fig. 5. The vorticity contours also show a rounder vortex for the experimental PIV data as compared to the oblong vortex seen in the CFD contours. Overall the streamwise vorticity contours for the 10° case compare better with the experimental results than the 23° case.

The contours for the 10° vane case are shown in Fig. 9 where the velocity and vorticity contours between the experiment and simulation compare better than the 23° vane case. There is a small difference in the streamwise velocity at the $15.2\,cm$ and $27.9\,cm$ downstream locations but overall the velocity contours compare well. The vorticity contours in Fig. 9 do show a more concentrated vortex at the $15.2\,cm$ and $27.9\,cm$ locations for the experiment as would be expected knowing the difference in the peak vorticity given in Fig. 5. The vorticity contours also show a rounder vortex for the experimental PIV data as compared to the oblong vortex seen in the CFD contours. Overall the streamwise vorticity contours for the 10° case compare better with the experimental results than the 23° case.

Turbulent Eddy Viscosity Effects

To better understand the difference between the numerical results using the SA and SST turbulent models, contour plots of the streamwise vorticity and the turbulent eddy viscosity are shown in Fig. 10. These contour plots show the streamwise vortex $15.2\,cm$ downstream from the trailing edge of the VG vane at $\alpha = 23°$. From the vorticity plots it can been seen that the simulation using the SST model has a much higher peak vorticity and thus a much more concentrated vortex. This concentration of the vorticity relates to the difference seen in the streamwise velocity contours. In an effort to explain this difference in the two turbulence models, a contour plot of the turbulent eddy viscosity, μ_t, which is generated by the turbulent models, are shown in Fig. 10. A comparison of these contours shows that the SA model generates a peak $\mu_t = 400$ very close to the core of the vortex. The SST model on the other hand shows a minimum μ_t near the center of the vortex. This could explain why the peak vorticity using the SA model is lower than the SST model. The higher value of μ_t will tend to dissipate the concentration of the vorticity thus reducing the peak vorticity of the vortex. The μ_t generated by the SST model does show a large zone just to the left of the vortex which may have a damping effect on the vortex. The distribution of the μ_t may also explain why the vortex in the numerical simulations are oblong and not circular as seen in the experimental PIV data.

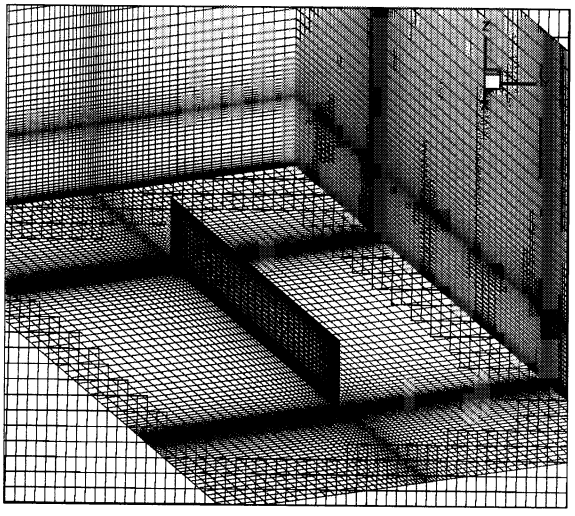

Fig. 11 Overset grids for the rectangular vortex generator vane.

Simplified Vane Geometry

Figure 11 shows a set of two grids which overlap and model a thin vane which has an area equal to the trapezoidal vane. This grid system does not account for the thickness of the vane but is much simpler to generate and can easily be modified to increase or decrease grid resolution. Comparisons between the thin vane model will be made to the

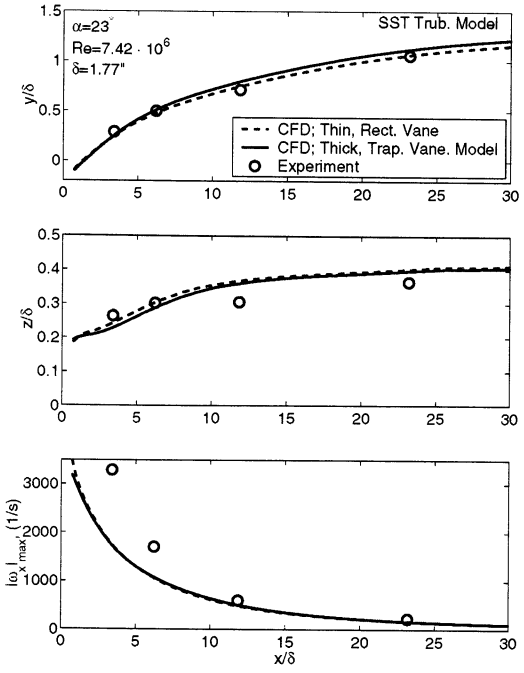

Fig. 12 Trajectory and magnitude comparisons of the peak streamwise vorticity, using the SST turbulence model, between the fully model trapezoidal vane and the rectangular thin vane at $\alpha = 23°$.

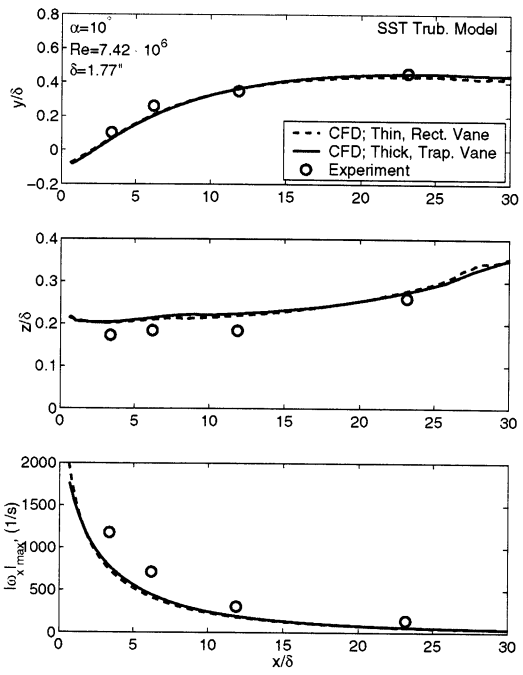

Fig. 13 Trajectory and magnitude comparisons of the peak streamwise vorticity, using the SST turbulence model, between the fully model trapezoidal vane and the rectangular thin vane at $\alpha = 10°$.

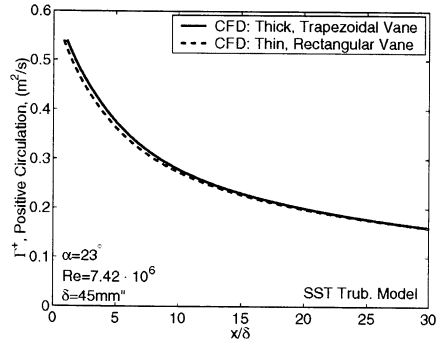

Fig. 14 Circulation comparison between the fully model trapezoidal thick, vane and the rectangular, thin vane at $\alpha = 23°$.

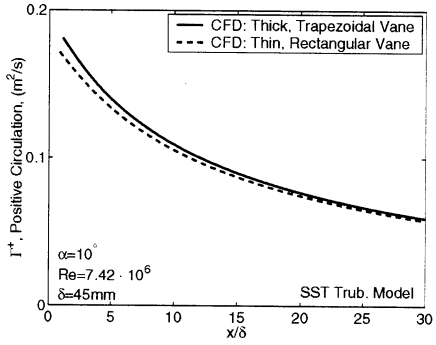

Fig. 15 Circulation comparison between the fully model trapezoidal, thick vane and the rectangular, thin vane at $\alpha = 10°$.

more complex trapezoidal vane.

To see how the simplification of vane geometry effects the streamwise vortex, a comparison between the fully modeled, thick trapezoidal vane, (shown in Fig. 1) was made to the thin rectangular vane (shown in Fig. 11). The dimensions of the rectangular vane were chosen such that the trapezoidal and rectangular vanes would have the same height with equal areas. Thus the height of the thin rectangular vane was 10.2 *mm* and had a chord length of 59.4 *mm*. The thin rectangular vane simulations have the same flow conditions as the trapezoidal vane using the SST turbulence model with $\alpha = 23°$ and 10°. Figures 12 and 13 shows a comparison between the trajectory and peak vorticity for the thick trapezoidal vane and the thin rectangular vane at $\alpha = 23°$ and 10°, respectively. These figures shows how the thin rectangular vane model compares very well to the fully grided thick trapezoidal vane. There is a slight difference in the spanwise and vertical vortex location for the $\alpha = 23°$ case. However the decay of the peak vorticity for the two simulations are almost identical. Figures 14 and 15 show the positive circulation comparisons between the thick and thin vanes. These figures reveal how the strength of the streamwise vortex for the $\alpha = 23°$ case are almost the same where the positive circulation for the thin vane is slightly lower than the thick vane. Figure 15 shows that the strength of the thin vane for $\alpha = 10°$ is smaller than

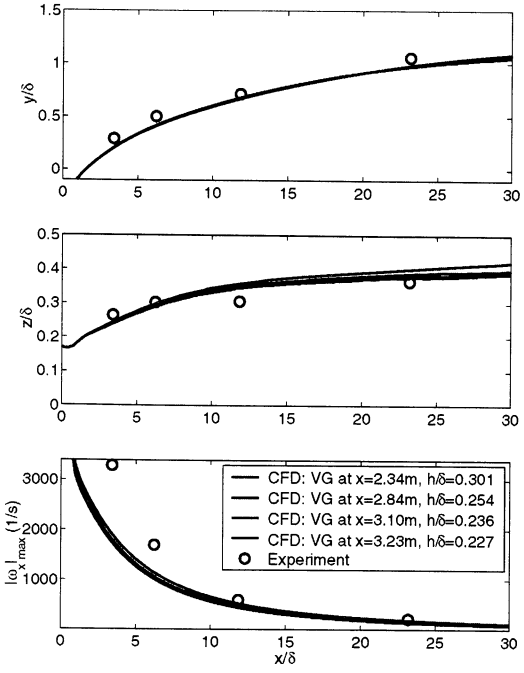

Fig. 16 Trajectory and magnitude comparisons of the peak streamwise vorticity, using the SST turbulence model, for four different vane locations where $\delta = 45mm$.

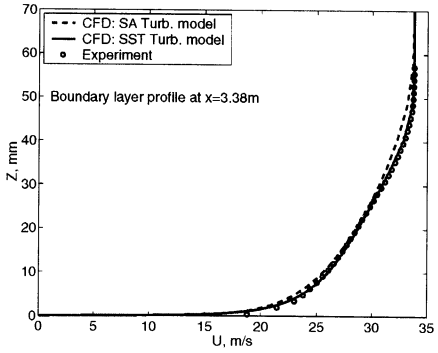

Fig. 17 Boundary layer profile for the baseline flat plate flow at $x = 3.38m$.

Table 1 A comparison of the peak vorticity $(1/s)$ between numerical simulations and experimental PIV data. The numerical simulations are performed by positioning the vane at the same locations on the flat plate as in the experiment showing the variance in the peak vorticity at a given distance downstream of the vane. The bold numbers in the CFD data correspond to the peak vorticity for the same vane location and downstream distance as performed in the experiment.

CFD Data	Distance downstream from vane, (cm)			
Vane Loc. (m)	15.2	27.9	53.3	104
x=2.34	1911	1143	527	**190**
x=2.84	1804	1060	**476**	163
x=3.10	1764	**1030**	457	153
x=3.23	**1745**	1016	448	148
Exp. Data	3290	1700	600	224

the thick vane for short distances downstream from the vane location but then improves for distances farther downstream. Overall the thin vane compares very well with the fully modeled thick trapezoidal vane. The thin vane grids have approximately 230,000 grid points as oppose to the fully modeled vane which has over 1.5 million grid points. Considering the small differences in the trajectory of the streamwise vortex between the thin rectangular vane and the fully grided trapezoidal vane, it would seem more cost effective to use the simplified thin vane grids rather than the fully modeled trapezoidal vane.

Effects of Boundary Layer Height

As a result of the fixed PIV measurement location, the vane was moved to different distances upstream in order study the evolution of the embedded vortex. Figure 3 shows the scaled drawing of the four different vane locations with respect to the baseline boundary layer thickness, δ, and the PIV measurement location. Since the vane geometry was held constant during the experiments, the vane height to boundary layer thickness ratio varies as the vane is moved to different locations along the flat plate. At the most upstream location, $h/\delta = 0.30$, and at the farthest downstream vane position, $h/\delta = 0.23$. In order to get an estimate of this effect on the experimental data, four numerical simulations were performed positioning the vane in the same locations as in the experiments. The trajectory and peak vorticity of the streamwise vortex from these simulations are shown in Fig. 16 where x/δ is the distance downstream from the trailing edged of the vane. These numerical simulations used the rectangular vane grids at $\alpha = 23°$ with the SST turbulence model.

From Fig. 16 it can be seen that there are small differences in the trajectories and peak vorticity decay rates. The spanwise trajectory for the four different vane locations show only a very slight difference. The vertical position of the vortex core does show a variation of the core height. This difference is very small for short distances downstream from the vane and becomes larger for longer distances. Since the vortex size will grow with the boundary layer thickness, this variation could be related to the boundary layer growth rate which is greatest for the most upstream vane position.

The plot of the peak streamwise vorticity does show larger values for the most upstream vane. However the differences between the experimental data and numerical simulations for the peak vorticity are much greater than the differences in vane location for distances less than $x/\delta = 10$. Also since the numerical simulations that were used to compare with the experimental data are for a vane at $x = 2.23\ m$, the first data point $15.2\,cm$ downstream from the vane, exactly matches the experimental vane location on the flat plate. As the data points become farther downstream from the vane, the h/δ ratio between the exper-

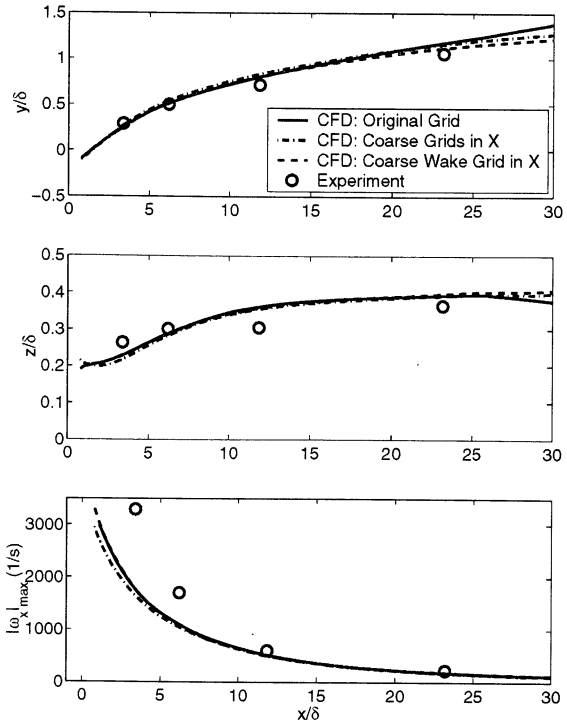

Fig. 18 Grid convergence of the wake and vane grids in the streamwise direction. The wake grid which captures the vortex from the vane grids is coarsen in the streamwise direction, x, using the original vane grids. This shows that the original numerical simulation is independent of the wake grid resolution in x. The second simulation show the results from halving all of the original grids in the x direction. This simulation shows a small decreases in the peak vorticity but no significant change in the vortex trajectory. These simulations were performed using the fully modeled trapezoidal vane grids at $\alpha = 23°$.

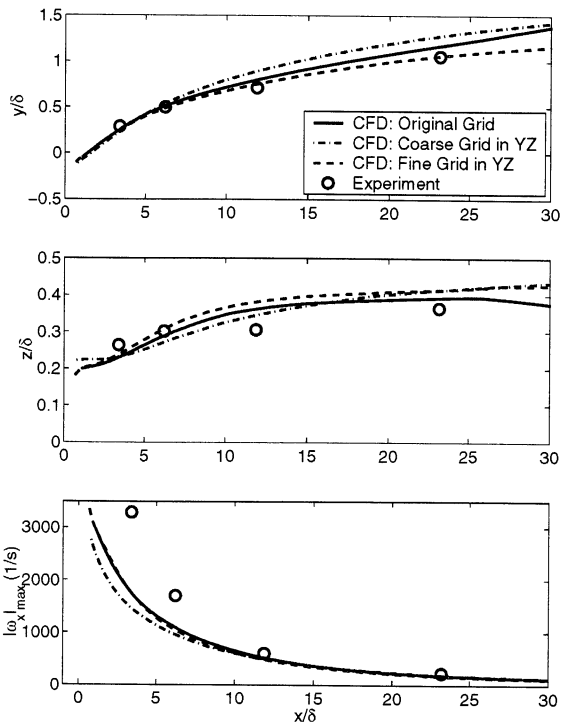

Fig. 19 Grid convergence of the wake grid in the cross-stream direction This figure shows how halving the number of grid points in the cross-stream direction produces a drop in the peak vorticity. Doubling the number of grid points in the cross-stream direction results in the peak vorticity remaining the same. Both the coarse and fine grids in the cross-stream direction show a small difference in the trajectory of the streamwise vortex. In the fine grid simulation the wake grid was coarsen in the streamwise direction. These simulations were performed using the fully modeled trapezoidal vane grids at $\alpha = 23°$.

iments and numerical simulations becomes greater. Table 1 shows the peak vorticity for the numerical simulations for the four vane locations along with the peak vorticity for the experiment. The bold values in the CFD data are the values which correspond to the numerical simulations which exactly match the experimental setup for that data point. This table shows that the first three data points downstream from the vane show only a small difference between the bold values and the $x = 3.23\,m$ values used in the previous comparison between CFD and experiment. The most significant difference is seen in the last data point, $104\,cm$ downstream from the vane. Since the vortex has almost diminished by this distance it can be argued that this difference becomes less significant. In summary, the error is small when comparing a numerical simulations of the streamwise vortex with the vane fixed at $x = 3.23\,m$, to the experimental results were the data measurement location is fixed and the vane is moved. More specifically the error for distances less than $27.9\,cm$ downstream from the vane are less than 1.5% and are shown to be as high as 6% at $53.3\,cm$ downstream. The farthest downstream data point location, $104\,cm$, does show a 22% error but at this distance the peak vorticity has decrease by 90% and the vortex has become very weak.

Boundary Layer Profile

One of the potential reasons for the difference between the peak vorticity between the numerical simulations and the experimental results could be the boundary layer profile. Since the vane is embedded in the boundary layer any difference in the boundary layer profile would result in more or less momentum seen by the vane which could result in a stronger or weaker vortex. A comparison between the boundary layer profile, at $x = 3.38\,m$, of the numerical simulation to the experimental data is shown in Fig 17. This figure shows the boundary layer profiles for the numerical simulations using the SA and SST turbulence models. From this figure it can be seen that the SST profile matches the experimental data very well. The velocity profile generated using the SA turbulence model also matches fairly well to the experiment but not as well as the SST

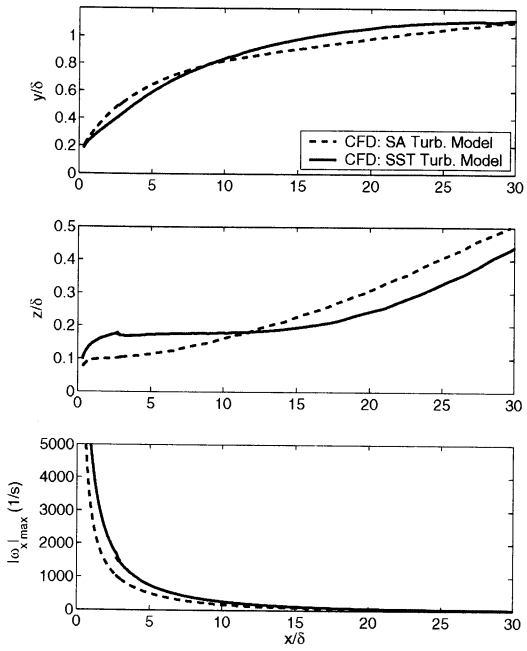

Fig. 20 Trajectory and magnitude comparisons of the peak streamwise vorticity, using the SA and SST turbulence models for the vortex generating jet simulations.

model. This comparison shows that the boundary layer profiles are predicted very well by the numerical simulations and are not a source for the large discrepancy between the peak vorticity observed between the experiment and numerical simulations.

Grid Convergence

The grid sensitivity of the embedded streamwise vortex is explored by comparing the trajectory results for coarse and fine grids. The grid resolution in the streamwise direction was evaluated first by comparing the previously computed results to those using a coarse and fine grid in the streamwise direction. The coarse grid was generated by halving the number of grid points in the streamwise, x, direction. Figure 18 shows the trajectory and peak vorticity from simulations where the wake grid was coarsen in the x direction and then a simulation where all of the grids were coarsen in the x direction. From this comparison it can be seen that when the wake grid is coarsen to 101 points in the streamwise direction, as compared to the original 301 points, that there is very little change in the vortex trajectory and peak vorticity. However, when all of the grids are coarsen in the x direction there is a small drop in the peak vorticity and very little change in the path of the vortex center. This shows that the original simulation results are converged as far as the streamwise grid resolution is concerned. These results also show that the original wake grid resolution in the x direction can be reduced without loss of resolving the vortex peak vorticity magnitude and trajectory.

Next the grid sensitivity of the streamwise vortex in the

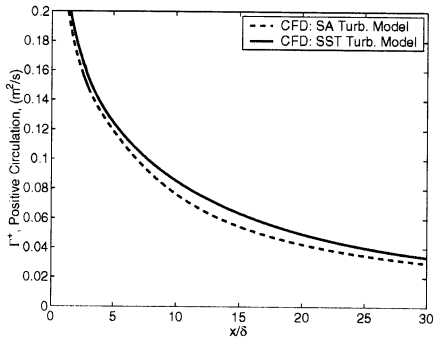

Fig. 21 Positive circulation for the vortex generating jet using the SA and SST turbulence models.

cross-stream direction was evaluated. As in the previous case, the original numerical results were compared to the results using coarse and fine wake and vane grids. The coarse grids were generated by halving the number of grid points in the vertical, z, and spanwise, y, directions. Likewise, the fine wake grid was generated by doubling the number of grid points in the z and y directions. Due to the large number of grid points need for this simulation, the wake grid for this case had the same number of grid points in the x direction as was used in the previous streamwise coarse wake grid. This was done since the vortex was not effected by coarsening the wake grid in the streamwise direction. Figure 19 shows a comparison between the coarse and fine grids simulations, in the yz plane, to the original simulation. This figure shows how the coarse grid simulation shows a small drop in the peak vorticity generated by the vane. It also shows a small difference in the trajectory of the vortex center. The simulation using the fine grids predicts the same peak vorticity with a small difference in the vortex trajectories. This result shows that the original simulation has been resolved in terms of the grid resolution in the cross-stream direction.

Vortex Generating Jet

The generation of a persistent streamwise vortex by a skewed jet was suggested by Pearcey[14] and later explained in more detail by Pearcey et al.[15] A vertical poster jet will generate two equal but opposite signed vortices on either side. When the jet is skewed, the vortex on one side of the jet is strengthened while weakening the vortex on the opposite side. The freestream flow then deflects the vortex generated by the jet aligning it with the freestream.

Using the nozzle grid shown in Fig. 2 where the jet is skewed 90^o to the freestream and pitched 15^o to the surface. The vortex generating jet has steady blowing with a velocity ratio, $VR = 4$ and a nozzle diameter of $1.36mm$. This simulation has periodic boundary conditions in the spanwise location which simulates an infinite row of jets with $52mm$ spacing. The simulation used a freestream velocity of $34m/s$ with a Reynolds number, $Re_L = 7.2 \cdot 10^6$, based on $L = 3.23m$, the length from the leading edge of the flat plate to the jet location.

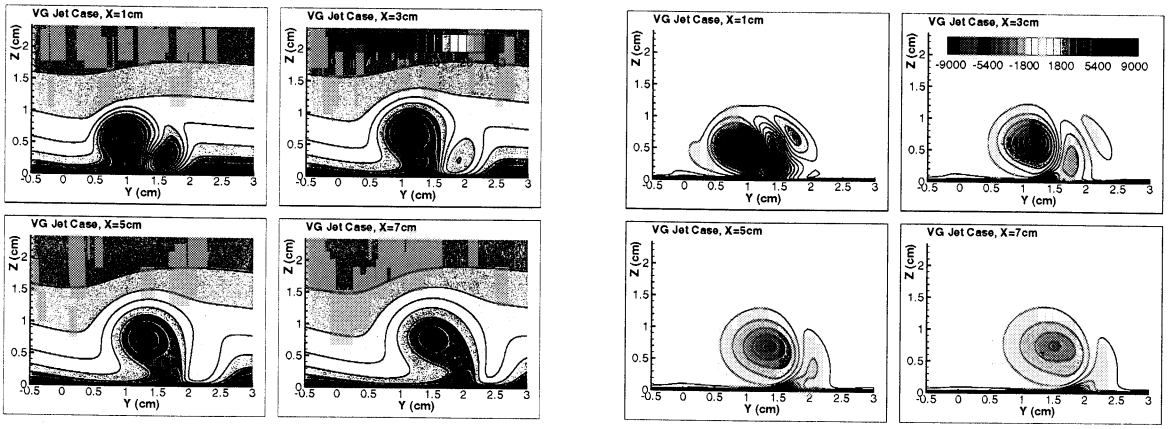

a) Streamwise Velocity

b) Streamwise Vorticity

Fig. 22 Contour plots of the streamwise velocity and vorticity VG jet, using the SST turbulence model, at four locations downstream of the jet.

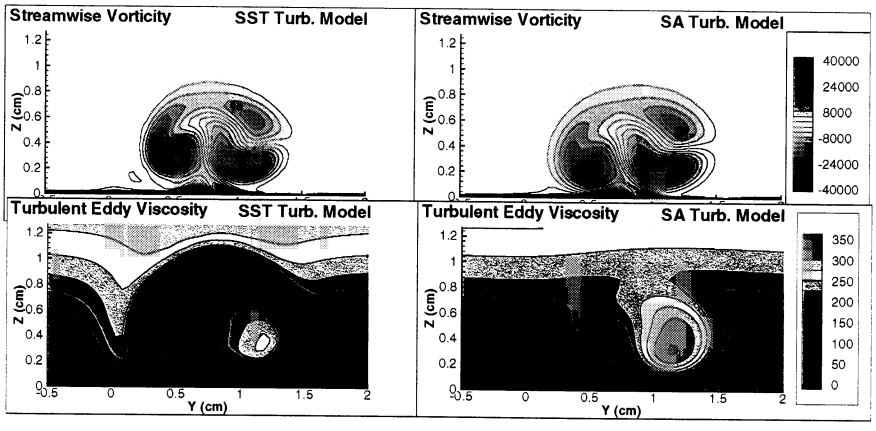

b) Eddy Viscosity

Fig. 23 Contour plots of the streamwise vorticity and the turbulent eddy viscosity, μ_t for the VG jet using the SA and SST turbulence models. Contours are taken $5.6mm$ downstream of the VG jet center.

The trajectory of the streamwise vortex generated by the skewed jet is shown in Fig. 20. This figure compares two numerical simulations using the SA and SST turbulence models. As was seen in the VG vane simulations, the SA turbulence model shows a lower peak vorticity at the core of the streamwise vortex. Figure 20 shows a small difference in the spanwise trajectory of the vortex between the two turbulence models. There is also a significant difference in the vertical trajectory of the vortex between the SA and SST turbulence models.

Figure 21 shows a comparison of the positive circulation for the SA and SST turbulence models. This figure shows that the strength of the vortex for the SA model is slightly lower than the vortex predicted using the SST model. Initially the vortex strength is about the same up to $x/\delta = 5$ and then the strength of the vortex using the SA model starts to decay faster than the SST model.

The streamwise velocity and vorticity contours a short distance downstream from the VG jet are shown in Fig. 22. The center of the jet is located at $y = 0$ and is blowing in the positive y direction. The contour plots show the streamwise velocity at $x = 1\,cm$ where a low velocity region, associated with the main vortex, can be seen. This contour plot also shows a high streamwise velocity region related to the jet core which has turned 90° and is aligned with the freestream flow. The streamwise vorticity contours show this high velocity region to be associated with the negative secondary vortex. This high velocity region is quickly damped out and can not be seen in the velocity contours at $x = 5\,cm$. Similarly the negative secondary vortex in this high velocity region decays rapidly as seen in Fig. 22.

Figure 23 shows the contours of the turbulent eddy viscosity generated by the two models along with the streamwise vortex contours. These contour plots are taken $5.6\,mm$ downstream from the center of the VG jet where the secondary negative streamwise vortex is just as strong as the primary positive vortex. From the contour plots of μ_t it can be seen that both turbulence models have a large μ_t near the secondary vortex. This increase of μ_t near the secondary vortex core could explain why this vortex decays in

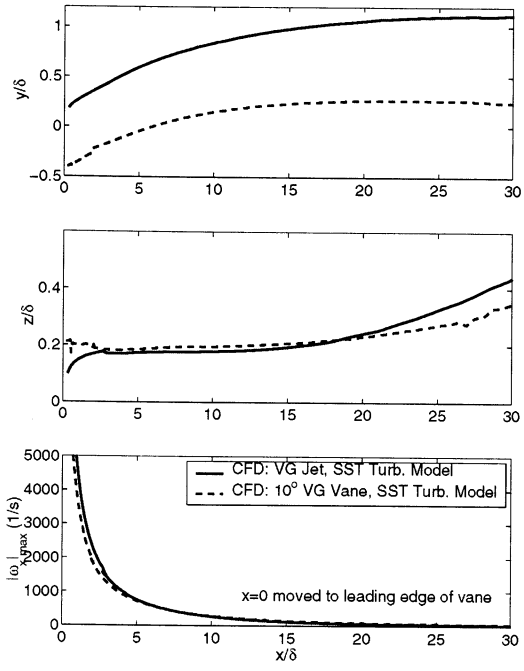

Fig. 24 Trajectory and magnitude comparisons of the peak streamwise vorticity, using the SST turbulence model, between the vortex generating jet and 10° vane simulations.

such a short distance. It's interesting to note that the SA model shows a higher peak μ_t near the secondary vortex when compared to the SST model. Near the primary vortex the μ_t levels are much lower where the SA model has a higher μ_t when compared to the SST model. As in the VG vane simulations, this higher μ_t generated by the SA model near the center of the primary vortex explains the lower peak vorticity when compared to the SST model.

The trajectory of the vortex generated by the jet is compared to the 10° vane vortex in Fig. 24. This comparison shows that the spanwise trajectory of the two vortices are very similar. The origin for this plot is located at the trailing edged of the vane and at the center of the jet orifice. The vane generates the vortex on the side of the vane which shows up as an offset when compared to the VG jet vortex. The vertical location of the jet vortex compares very well to the vane vortex. The peak vorticity trajectories between the VG jet and vane are shown to be very similar. Figure 25 shows a comparison of the positive circulation between the VG jet and the 10° vane. This figure shows that the strength of the 10° vane vortex is greater than vortex generated by the jet. Both vortices show a similar rate of decay of the positive circulation for distances greater than $x/\delta = 10$. The difference in the initial decay of the positive circulation is most likely related to the negative secondary vortex generated by the VG jet. Figure 26 shows the streamwise velocity and vorticity contours at the same contour levels and locations as the 10° vane case shown in Fig. 9. A comparison between these two figures shows how the flow patterns between the jet and vane look very similar.

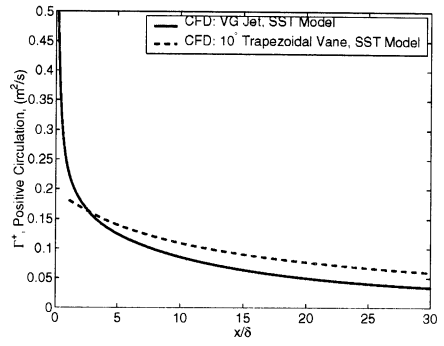

Fig. 25 Positive circulation for the vortex generating jet compared to the 10° vane, using the SST turbulence model.

Summary

The ultimate goal of this investigation is to obtain a better understanding of the physics of a low-profile vortex generating vane and jet. The numerical simulations of the fully modeled vortex generating vane and jet will then be used in the future development of a reduced CFD model. Simulations of the vortex generating vane and jet, submerged within a turbulent boundary layer flow over a flat plate, were performed using a RANS flow solver. The vortex generating vane simulations were then compared to experimental wind tunnel stereo digital particle image velocimetry data. From this comparison the trajectory of the streamwise vortex in the spanwise and vertical directions showed good agreement between the numerical simulations and experiments. A comparison of the peak vorticity, which is an indication of the vortex concentration, was under predicted by the RANS flow simulations. However a comparison of the positive circulation, which indicates the vortex strength, showed that the CFD and experiments agreed well except for short distances downstream of the vanes. This comparison of the circulation and peak vorticity for the vane cases showed that the numerical simulations were able to predict the strength of the streamwise vortex but would diffused the vortex much faster than was observed in the experiments.

A comparison between two turbulence models for the vane case showed that the SST turbulence model was able to predict the vortex trajectory and peak vorticity decay rate much better than the SA turbulence model. The prediction of the flow for the vane at 10° was much better than the 23° case where the difference between the SA and SST models were smaller. The turbulent eddy viscosity, μ_t, generated by the turbulence models shows the SA model having a peak μ_t near the center of the vortex where the SST model shows a minimum μ_t. This difference in the turbulent eddy viscosity would explain why simulations using the SA turbulence model displayed a more diffused vortex. The positive circulation comparisons showed that both simulations using the SA and SST turbulence models generated a streamwise vortex of equal strength. This shows that the differences in the peak vorticity between the turbulence models are related to the diffusion of the vortex and

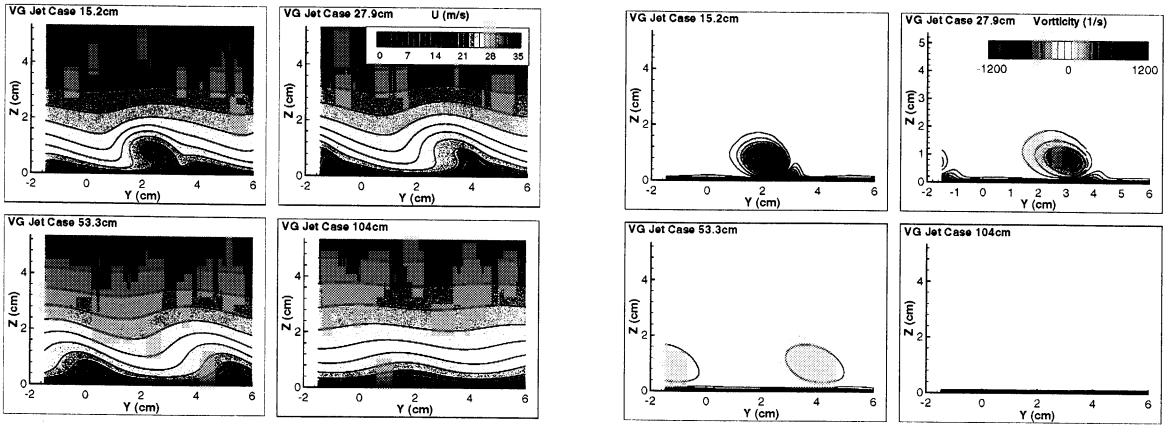

a) Streamwise Velocity

b) Streamwise Vorticity

Fig. 26 Contour plot of the streamwise velocity and vorticity for the VG jet using the SST turbulence model at four different locations downstream of the jet.

not the initial strength.

A grid convergence study for the vane case did not show any improvements in the diffusion of the streamwise vortex, showing that the diffusion of the vortex was not related to grid resolution. These results point toward the numerical scheme and the turbulence modeling as the probable source for the increased vortex diffusion seen in the numerical simulations when compared to the experiments.

The simulation of a simplified rectangular thin vane was compared to a fully modeled trapezoidal vane of finite thickness. This comparison showed that the rectangular vane produced a streamwise vortex which was very similar to the fully grided vane. A comparison of the positive circulation also showed that they both generated streamwise vortices of equal strength. Therefore the fully grided trapezoidal vane could be replaced by a more simply grided thin vane.

Simulations of a vortex generating jet showed that the SST turbulence model resulted in higher peak vorticity values when compared to simulations using the SA turbulence model. A comparison between the vortex generating jet and the 10° vane showed that they had similar trajectories and peak vorticity decay rates. While the 10° vane had a stronger vortex both showed similar decay rates for the strength of the vortex. Unlike the vortex generating vane, the jet had a large negative secondary vortex, for short distance downstream from the jet. This secondary vortex decays rapidly resulting in a vorticity distribution whose structure becomes similar to the vortex generated by the 10° vane. These similarities show promise that a reduced CFD model for the VG vane could be used for the VG jet.

References

[1]Hamstra, J. W., Miller, D. N., Truax, P. P., Anderson, B. H., and Wendt, B. J., "Active inlet flow control Technology Demonstration," ICAS-2000-6.11.2, 22nd International Congress of the Aeronautical Sciences, Harrogate, UK, 2000.

[2]Bender, E. E., Anderson, B. H., and Yagle, P. J., "Vortex generator modeling for Navier-Stokes codes," FEDSSM99-6919, 3rd Joint ASME/JSME Fluids Engineering Conference, San Francisco, CA, 1999.

[3]Buning, P. G., Jespersen, D. C., Pulliam, T. H., Klopfer, W. M., Chan, W. M., Slotnick, J. P., Krist, S. E., and Renze, K. J., "OVERFLOW user's Manual Version 1.8m," Tech. rep., NASA Langley Research Center, 1999.

[4]Jespersen, D. C., Pulliam, T. H., and Buning, P. G., "Vortex generator modeling for Navier-Stokes codes," AIAA 97-0644, 1997.

[5]Pulliam, T. H. and Chaussee, D. S., "A Diagonal Form of an Implicit Approximate-Factorization Algorithm," *Journal of Computational Physics*, Vol. 39, February 1981, pp. 347–363.

[6]Steger, J. L., Dougherty, F. C., and Benek, J. A., "A Chimera Grid Scheme," *Advances in Grid Generation*, edited by K. N. Ghia and U. Ghia, Vol. 5 of *FED*, ASME, New York, NY, 1983.

[7]Spalart, P. and Allmaras, S., "A One-Equation Turbulence Model for Aerodynamic Flows," *La Recherche Aerospatiale*, , No. 1, 1994, pp. 5–21.

[8]Menter, F., "Improved Two-Equation Turbulence Models for Aerodynamic Flows," Tech. Rep. TM 103975, NASA, NASA Langley Research Center, Hampton, VA 23681-2199, 1992.

[9]Jespersen, D. C., "Parallelism and OVERFLOW," Tech. Rep. NAS-98-013, NASA, NASA Langley Research Center, Hampton, VA 23681-2199, October 1998.

[10]Chan, W. M. and Gomez, R. J., "Advances in Automatic Overset Grid Generation Around Surface Discontinuities," AIAA Paper 99–3303, July 1999.

[11]Yao, C. S., Lin, J. C., and Allan, B. G., "Flowfield Measurement of Device-Induced Embedded Streamwise Vortex on a Flat Plate," AIAA Paper 02–3162.

[12]Lin, J. C., "Control of turbulent boundary-layer separation using micro-vortex generators," AIAA 99–3404, 1999.

[13]Lin, J. C., Howard, F. G., and McGhee, R. J., "Small submerged vortex Generators for Turbulent Flow Separation Control," *Journal of Spacecraft and Rockets*, Vol. 27, No. 5, Oct. 1990, pp. 503–507.

[14]Pearcey, H. H., "Shock Induced Separation and its Prevention by Design and Boundary Layer Control," *Boundary Layer and Flow Control*, edited by G. V. Lachman, Pergamon Press, Oxford, 1961.

[15]Pearcey, H. H., Rao, K., and Sykes, D. M., "Inclined Air-Jets used as Vortex Generators to Supress Shock-Induced Separation," Tech. Rep. CP-534, Paper 40, AGARD, April 1993.